molecules

MDPI

Article

Synthesis and Characterization of Na-P1 (GIS) Zeolite Using Rice Husk

Daniela Novembre [1,*], Domingo Gimeno [2], Lucia Marinangeli [1], Anna Chiara Tangari [1], Gianluigi Rosatelli [1], Michele Ciulla [3] and Pietro di Profio [3]

[1] Dipartimento di Scienze, Università degli Studi "G. d'Annunzio", Via dei Vestini 30, 66013 Chieti, Italy; lucia.marinangelii@unich.it (L.M.); a.tangari@unich.it (A.C.T.); gianluigi.rosatelli@unich.it (G.R.)
[2] Department Mineralogia, Petrologia i Geologia Aplicada, Universitat de Barcelona, 08028 Barcelona, Spain; d.gimeno.torrente@gmail.com or domingo.gimeno@ub.edu
[3] Department of Pharmacy, University of Chieti-Pescara "G. d'Annunzio", Via dei Vestini, 66100 Chieti, Italy; pietro.diprofio@unich.it (P.d.P.)
* Correspondence: daniela.novembre@unich.it; Tel.: +39-3556153

Abstract: This work deals with the synthesis of Na-P1 (GIS) zeolite using rice husk as the starting material, instead of the more expensive chemicals currently used in the industry (i.e., Na aluminates and Na silicates). Rice husk is calcined at the temperature of 550 °C to obtain rice husk ash. Na-P1 is synthesized starting from rice husk ash, NaOH, and $NaAlO_2$ by a protocol involving the mixing of a seed gel and a feedstock gel. Two synthesis runs are carried out at ambient pressure at the temperature of 110 °C by fixing the SiO_2/Al_2O_3 ratio at 3.5 and 5.3, respectively. The synthesized products have been identified as well as the experiments developed by X-ray diffraction and scanning electron microscopy. Then, the most successful synthesized powders were also characterized by infrared spectroscopy, Raman spectroscopy, specific surface area (BET), and differential thermal analysis. The cell parameters are calculated using the Rietveld method. The combined Rietveld and reference intensity ratio methods allows us to exclude the presence of impurities and residual amorphous phase in the conducted experiments. Testing rice husk as a source of amorphous silica in the synthesis of Na-P1 represents both economic and environmental advantages. The high yields and the results of the experiment open the way for the transfer to an industrial production scale.

Keywords: rice husk; synthesis; zeolite Na-P1

Citation: Novembre, D.; Gimeno, D.; Marinangeli, L.; Tangari, A.C.; Rosatelli, G.; Ciulla, M.; di Profio, P. Synthesis and Characterization of Na-P1 (GIS) Zeolite Using Rice Husk. *Molecules* **2024**, *29*, 5596. https://doi.org/10.3390/molecules29235596

Academic Editor: Wenfu Yan

Received: 15 November 2024
Revised: 23 November 2024
Accepted: 25 November 2024
Published: 26 November 2024

1. Introduction

Although zeolites constitute a group of natural tectosilicates that have been known since the mid-18th century, and some of their properties began to be known a century later, it was only in 1948 when Union Carbide began to synthesize them with industrial objectives that awareness of them developed exponentially. Today, we know about 100 naturally occurring minerals with synthetic analogs now reaching more than 250 species. As is well knowledge of these minerals, the crystallochemistry of these types of tectosilicates is characterized by three-dimensional frameworks of Al/Si tetrahedra linked by sharing their oxygen atoms to form channels containing water and exchangeable alkaline or alkaline earth cations. These structural characteristics give them various properties such as ion exchange capability, solid acidity, adsorption, and catalytic capabilities, a fact that has allowed a large number of industrial uses to be discovered and initially promoted before the synthesis of new mineral species as well as cost optimization strategies for these syntheses. Referring to the latter, the optimization of processes are mainly channeled into shorter, simpler, and less energy-consuming times and processes, and the use and enhancement of waste or by-products from other industrial processes.

The zeolite GIS class has the typical oxide formula: $M_{2/n}O{\cdot}Al_2O_3{\cdot}1.80–5.00SiO_2.5H_2O$ where M is a n-valent cation, normally an alkali metal [1]. The sodium P zeolites are classified as synthetic counterparts of Gismondine-type (GIS) and their smaller micropore size (~2.9 Å) makes them useful and valuable applicants for the water vapor adsorption and separation of small molecules [2]. Albert et al. [3] indicate these zeolites as the most open framework-type generated thus far owning to the high flexibility of the Si-Al linkage.

Four different polymorphs have been recognized due to variable Si/Al ratio: the cubic phase called Na-P1, refined in $I4_1/AMD$ [4]; the orthorhombic phase—the so-called Na-P2 crystallizing in *Pnma* [5]; the tetragonal phase for high silica variety of Na-P refined in $I4_1/AMD$ [6]; and the monoclinic phase for P with a strict Si/Al ratio of 1.0 [3].

P zeolites are successfully used in water-softening [7], as components of environmentally friendly detergents [8], as sorbents of heavy metals [9], in gas separation applications [6], for the removal of radioactive waste species [1,8,10,11], and as stable support to prevent agglomeration in dispersing of particles in aldol condensation of cyclohexanone with benzaldehyde [12,13].

The standard procedure from the International Zeolite Association Synthesis Commission (IZA) is the hydrothermal method which indicates long crystallization times of 60 days [14].

Zeolite P has been synthesized in the past not only using the hydrothermal method [1,3,5,8,15–17], but also the microwave technique [18,19], the sol–gel process [20] and the sonochemical method [21].

The synthesis from low-cost silica-alumina sources has also been explored involving the use of fly ash [22–25], kaolinite [26], clays [20,27], nuclear wastes [28], waste glasses [29], transformation of natural mordenite and clinoptilolite [30–32], and rice husk silica [33–38].

With regard to the use of rice husk ash (RHA), Khabuanchalad et al. [33] reported the partial transformation of Y zeolite, synthesized from RHA, in NaP after a 5-day crystallization time; also, Wittayakun et al. [34] synthesized NaY from RH at 90 °C obtaining NaP as an additional product. Mohamed et al. [35] used RH to synthesize NaY obtaining a mixed intermediate product of NaY and NaP after mixing the seed gel and the feedstock gel at 110 °C for 24 h. Kongkachuichay and Lohsoontorn [36] used perlite and RH to synthesize analcime, Na-P1, and sodalite; RH was burned at 700 °C and the experiments were carried out in an autoclave with SiO_2/Al_2O_3 molar ratios of 1 to 40, NaOH concentrations of 1 to 4 N, and starting pressure of 1 atm; the existence field of Na-P1 as the isolated phase is related to NaOH concentrations below 1.5 and to SiO_2/Al_2O_3 molar ration between 5 and 9 at 140 °C. However, it must be said that an X-ray pattern, which testifies to the sole presence of the phase as a synthesis product, is neither provided nor other types of spectroscopic characterizations performed for the NaP zeolite. Furthermore, a cumulative characterization of the specific surface area and pore size is carried out without distinguishing between analcime, NaP, and sodalite. As far as the morphology of crystals is concerned, the authors generically indicate NaP as aggregates of various shapes. Referring to this point it should be said that Huo et al. [8] also reported the synthesis of NaP with different morphologies/crystalline habits. These authors synthesized NaP starting from chemical reagents and conducted a study aimed to define the influence of the SiO_2/Al_2O_3 ratio in determining the shape of crystals.

The scope of the present work is to test RHA in the synthesis of high-purity monomineralic powders of Na-P1 (i.e., producing Na-P1 crystals characterized by a distinct morphology and homogeneous crystal size), working on the reduction in both the calcination and synthesis temperatures and the synthesis times and improving the degree of crystallinity of the synthesized powders (i.e., in terms of absence of amorphous phase and/or impurities coming from the raw material). Kongkachuichay and Lohsoontorn [36] state that zeolites are accompanied with trace amounts of unreacted perlite; at the same time, they define the synthesized zeolite as "pure" simply by comparing the peak positions to those of a collection of simulated XRD powder patterns of zeolites [39].

Furthermore, the work includes a quantitative phase analysis (combining Rietveld and reference intensity ratio methods) and a morphological, physical, and spectroscopic characterization for the Na-P1 zeolite obtained from RHA is provided here for the first time.

2. Results and Discussion

The result of Powder X-Ray Diffraction analysis (PXRD) performed on RHA (Figure 1) reveals the amorphous character of the material (Figure 1a); a bulge around 20° 2 theta is in fact evidenced and indicative of non-crystalline material.

Infrared (IR) analysis was conducted on RHA (Figure 1b). It results in a strong band at 1074 cm^{-1} related to the asymmetric stretching vibrations of tetrahedral SiO_4. A second minor band is located at 800 cm^{-1} associated with the symmetric stretching of SiO_4 tetrahedra. The third strong and narrow band at 465 cm^{-1} is due to Si-O bending. The results agree with Petkowicz et al. [40], Yusof et al. [41], and Novembre et al. [42].

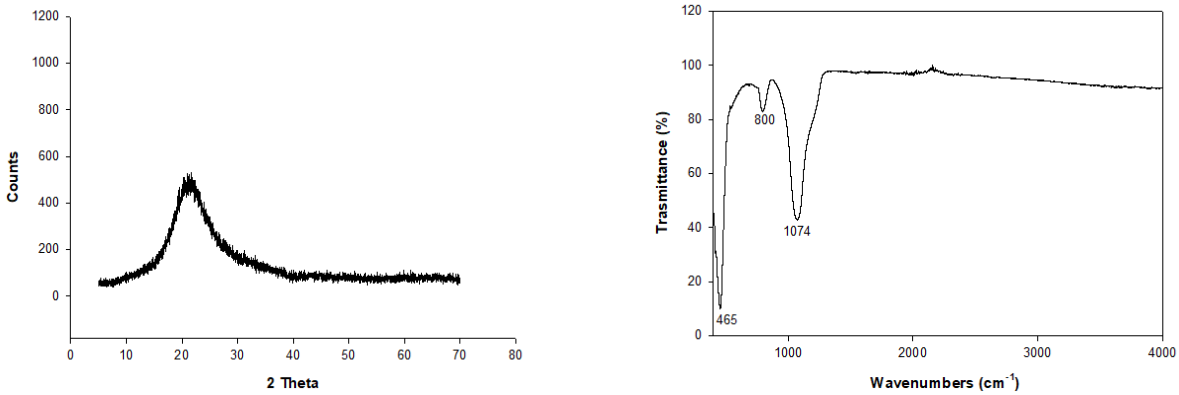

(**a**) (**b**)

Figure 1. (**a**) X-ray spectra of RHA. (**b**) IR analysis on RHA.

The percentage of the chemical composition of RHA determined by XRF is reported in Table 1, indicating a silica content of 98.55% and minor amounts of other oxides.

Table 1. Percentage of chemical composition of RHA determined by XRF.

SiO_2	Al_2O_3	Fe_2O_3	CaO	Na_2O	K_2O	MnO	TiO_2	MgO	P_2O_5
98.55	0.28	0.16	0.16	0.18	0.22	0.16	0.02	0.14	0.13

The synthesis runs conducted at 110 °C for experiments A and B are illustrated in Figure 2a,b. The appearance of Na-P1 zeolite is evident at 33 h for both the experiments. The reflection intensities increase reaching their maxima at 48 h. Comparing the two synthesis runs, it can be noted that the zeolitic crystallization seems to proceed at a greater speed in experiment B, as shown by the intensities of the counts at 33 h. It should be noted, however, that the intensities of the counts at the end of the runs appear comparable.

On the other hand, substantial differences in the morphologies of the crystals are highlighted through SEM analysis.

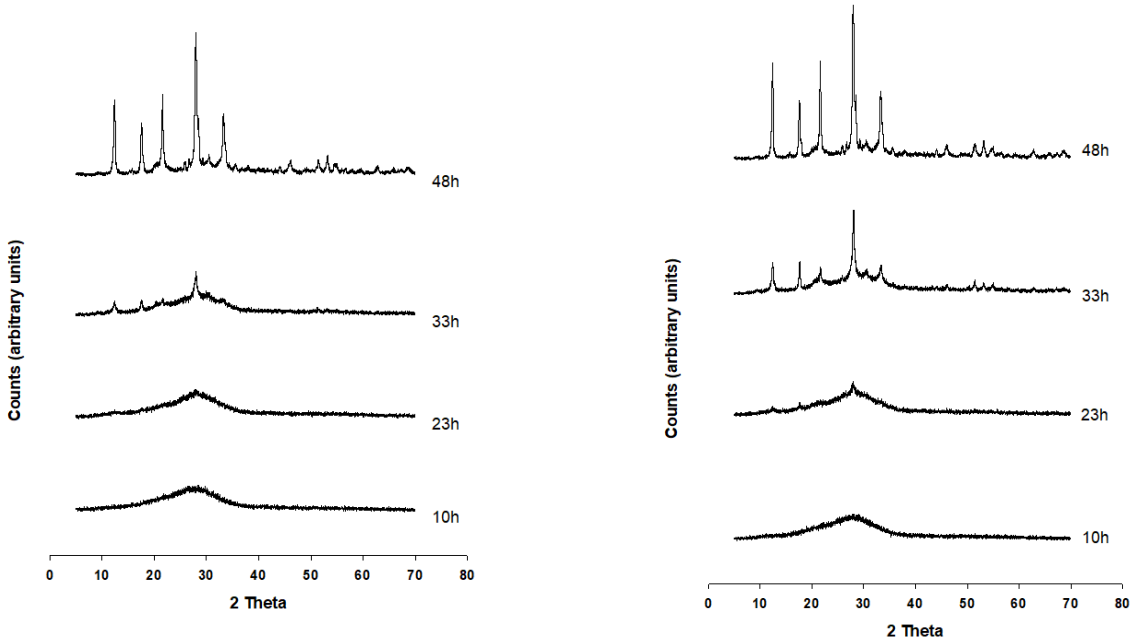

Figure 2. PXRD patterns of the synthesis run A (**a**) and B (**b**).

Figure 3a,b present SEM images of Na-P1 crystals from experiment A at 33 h and 48 h, respectively. It reveals a microsphere morphology of the crystals and an average maximum size of crystals around 2 microns.

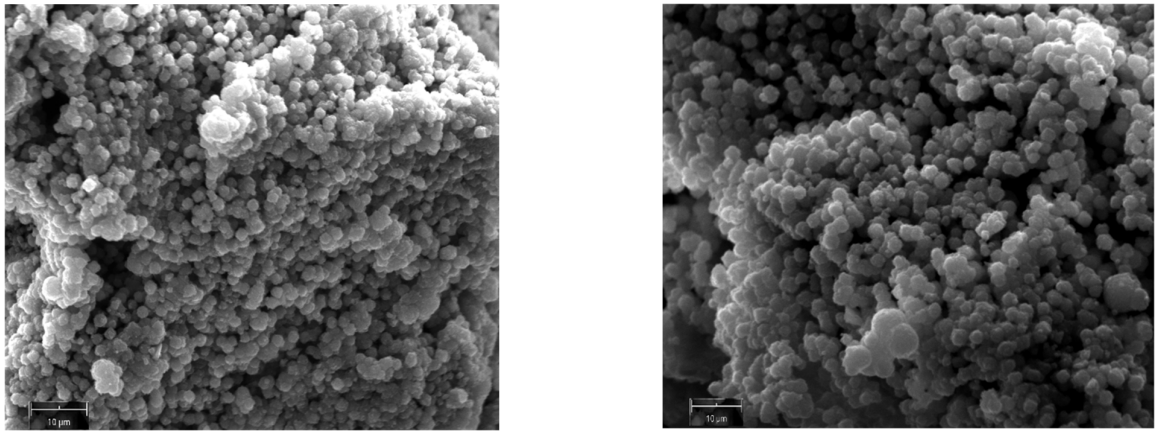

(**a**) (**b**)

Figure 3. SEM images of Na-P1 zeolite crystals obtained at 48 h (110 °C) for experiment A (**a**,**b**).

Figure 4a,b report SEM images of Na-P1 crystals from experiment B at 48 h. In this case, different sizes and morphologies emerge for Na-P1 crystals. Besides crystals characterized by a microsphere morphology (5–7 microns), there are also wool ball-like-shaped crystals (around 10 microns). Together with these two morphologies another one is visible, associated with smaller crystals of about 1–2 microns characterized by an angular, pseudo-octahedral morphology.

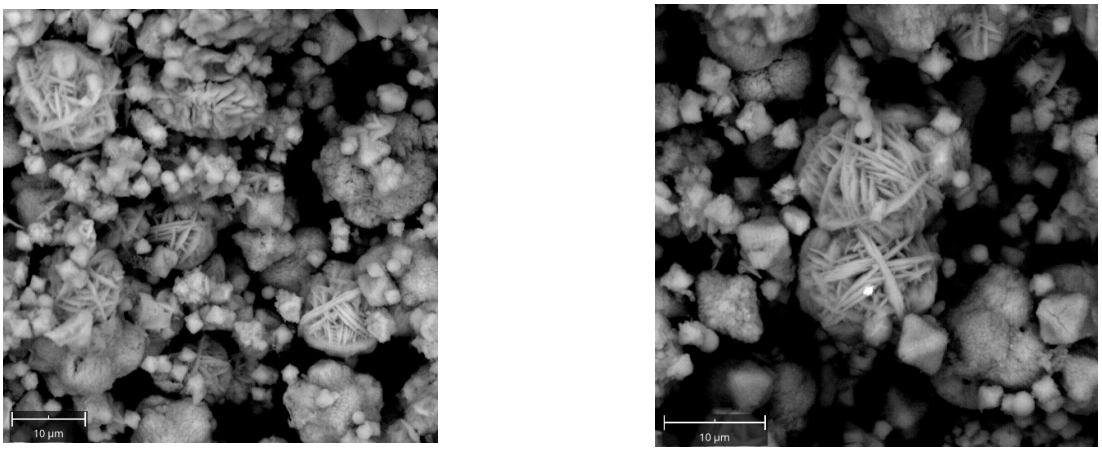

(**a**) (**b**)

Figure 4. SEM images of Na-P1 zeolite crystals obtained at 48 h (110 °C) for experiment B (**a**,**b**).

Huo et al. [8] reported the synthesis of zeolite NaP with controllable morphologies starting from commercial reagents, i.e., sodium hydroxide, sodium aluminate, and sodium silicate. The authors explain how the SiO_2/Al_2O_3 ratio plays an important role in morphology control. In particular, a mixture of different morphologies emerges for SiO_2/Al_2O_3 ratios between 5 and 10. Also, in our case, a microsphere morphology is observed for SiO_2/Al_2O_3 ratio of 3.5, while a coexistence of different morphologies is visible at the higher ratio of 5.3.

Given that the industrial processes require homogeneous products to perform chemical reactions with selected-sized molecules, we focused our attention on experiment A, which showed synthetic powders characterized by the presence of Na-P1 zeolite crystals of the same morphology and of dimensional homogeneity.

Further characterizations were therefore conducted on the sample produced at 48 h of experiment A.

The results of the QPA analyses are illustrated in Table 2.

Table 2. Results of the QPA analyses conducted on samples synthesized at 170 °C.

Sample + 10% Corundum Nist 676a	**110 °C-48 h**
R_{wp}	0.18
R_p	0.15
CHI^2	2.39
space group Na-P1	*C2/c*
a (Å)	14.3027 (0.0023)
b (Å)	10.0857 (0.0035)
c (Å)	10.0129 (0.0042)
β (°)	135.2833 (0.0031)
% amorphous	6.5 (15)
Na-P1	93.5 (18)

The observed and calculated profiles and difference plots for Na-P1 and corundum NIST 676a are reported in Figure 5. In particular, at 48 h, 93.5% of zeolitic phase is achieved. Cell parameters of Na-P1, refined with monoclinic symmetry space group *C2/c*, are reported in Table 2. The results of the Rietveld refinements provide cell values that are in good agreement with the structural model proposed by Albert et al. [3].

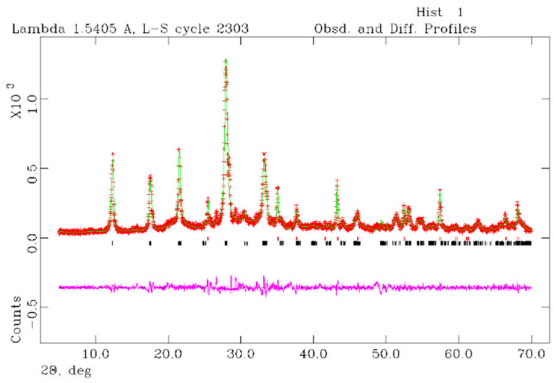

Figure 5. Rietveld refinement plot: observed (red +), calculated profiles (green) and difference plot (pink) for Na-P1 zeolite (110 °C-48 h) and corundum NIST 676a with tick marks at the position of the Bragg peaks. From the bottom: Na-P1 zeolite, corundum NIST 676a.

Using the BET method, the obtained zeolites had a specific surface area of 13.27 m^2/g and the average pore volume of 0.0071 cm^3g^{-1}. The specific surface area is rather small due to the low particle size of the sample, as confirmed by SEM analysis, and is also attributable to the fact that Na-P zeolite only has 8-membered rings in its structure, as previously observed by Breck, Huo, et al. and Ali et al. [8,14,43]. Figure 6 illustrates the nitrogen adsorption–desorption isotherms of the Na-P1 zeolite from experiment A. It results in a vertical hysteresis loop proving the existence of cylindrical mesopores in the zeolitic structure.

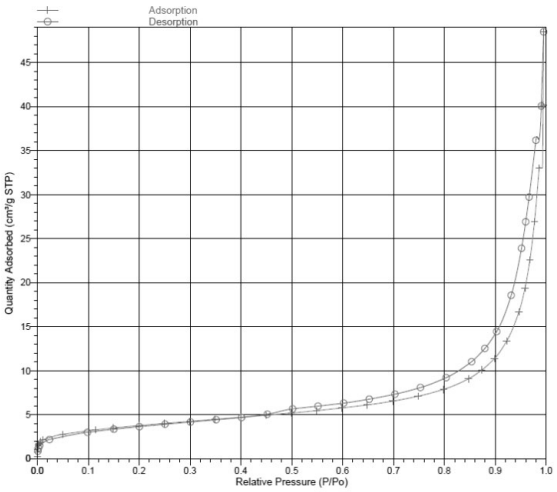

Figure 6. Nitrogen adsorption–desorption isotherms of the Na-P1 zeolite from experiment A.

Figures 7 illustrates the infrared spectrum. The significant broad peaks are located at 3402 and 1638 cm^{-1} for sample 6A-48 h-110 °C; these peaks are related to O-H stretching and bending, respectively. The band at 1096 cm^{-1} is assigned to the asymmetric stretching vibration due to external linkages between tetrahedra, structure sensitive, sensu Flaningen et al. [44], and that at 983 cm^{-1} is assigned to the asymmetric stretching vibration caused by internal vibrations of the framework SiO_4. The bands at 739 and 677 cm^{-1} are attributed to Si-O-Si symmetric stretching vibration of internal tetrahedron. The peak at 606 cm^{-1} is attributed to the double rings' vibration. Data are coherent with those available in the literature [8,14,44,45].

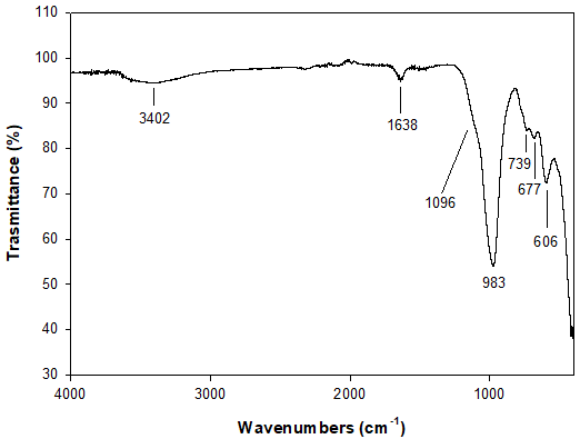

Figure 7. IR spectrum of the Na-P1 (48 h at 110 °C).

Figure 8 reports the Raman spectrum for the sample 6A-48 h-110 °C. It results in a peak at 392 cm^{-1} related to the vibration mode of Al-O-Al and a peak at 492 cm^{-1} associated with the vibration mode of Si-O-Si. These data are coherent with findings by Tsai et al. [46] that report the characteristic peaks in the region of 391–432 cm^{-1} and 463–497 cm^{-1} for the doubly connected four-ring chain of the Gismondine group. Also, Mozgawa [47] indicates the bands in the range of 470–520 cm^{-1} due to the "breathing" vibrations of the 4-membered rings. The peak at 212 cm^{-1} is assignable to the vibration mode of Na-O.

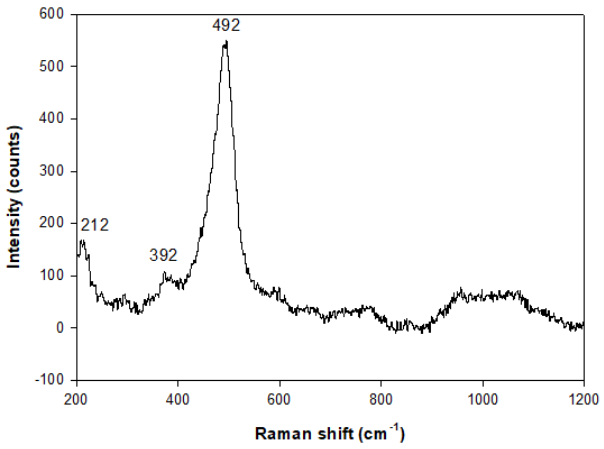

Figure 8. Raman spectrum of the sample at 48 h (110 °C) of experiment A.

Thermogravimetric analysis has revealed a gradual and continuous water loss up to 1000 °C (Figure 9). In particular, it indicates a two-stage mass loss. Physisorbed water is lost up to 120 °C. There also seems to be at least one more stage of water release between 110 and 150 °C which might be interpreted as evidence for the existence of two types of water molecules in the structure of different bound energies. C.a. 17% loss occurs at about 585 °C; between 585 ° and 900 °C a mass loss of 0.31% is registered and related to the removal of the crystal water. The endothermic peaks revealed by the DTA curve at 120 °C reflect the dehydration process and are in agreement with findings by Zubowa et al. and Huo et al. [8,18]. At about 838 °C there is an endothermic peak which testifies the melting of the phase.

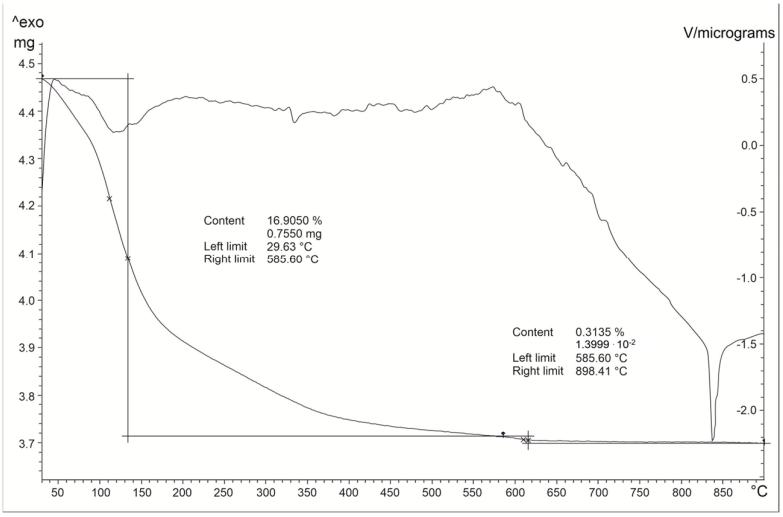

Figure 9. DTA-TG analysis of the sample at 48 h (110 °C) of experiment A. The asymptotic line to the x scale represents the TG analysis while the above line is related to DTA analysis.

3. Materials and Methods

Rice husk (RH) coming from a rice field on the northeastern coast of Spain underwent preliminary treatments: grinding, washing, and drying at 105 °C for 24 h. Then, calcination of RH was performed in an open porcelain crucible which was heated in a BE43N BICASA furnace (Bernareggio, Italy) to the calcination temperature of 550 °C at a pressure of 1 atm for 6 h; the heating rate of the sample was 1.5 °C s^{-1} [48,49]. Following the calcination treatment, RH ash (RHA) was obtained.

RHA composition was determined by X-ray fluorescence (XRF), with a WDXRF, Panalytical (Malvern, UK), Axios PW 4400/40 sequential spectrophotometer at the Centres Cientifics i Tecnològics de la Universitat de Barcelona (CCiT-UB). Major element determination has been carried out using fused pearls (lithium tetra borate pearls at a dilution of 1/20) according to the procedure by Novembre et al. [42,50], Gisbert and Gimeno [51], and Aulinas et al. [50]. In order to establish the XRF calibration curve, it is necessary to have a range of standards with a chemical composition similar to that of the unknown. Nevertheless, it is unusual to analyze materials with such a high silica content as RHA (and consequently it is not common to have standards for that composition). Therefore, an ad hoc procedure was developed to analyze ash with such a high silica content, i.e., mixing carefully 1:2 and 1:3 proportions of basaltic composition with RHA at international standards [52]; thus the final raw data resulted in the calibration range of the WDXRF for rhyolite-andesite. In the same way, taking into account the limitation of XRF methods in the calculation of Na in low contents, this fact was surpassed with an in-house laboratory calibration of raw data provided by WDXRF with inner standards and matrices of comparable composition, previously analyzed by AAS [53–55].

NaOH and $NaAlO_2$ were used in the synthesis protocol (Honeywell Riedel-de Haen, Bucharest, Romania, purity of 99%).

The seed gels were prepared by mixing the silicate solution with the aluminate one according to the following procedure: 1 g of RHA dissolved in 30 mL NaOH (8%) solution; 1.4 g of $NaAlO_2$ dissolved in 30 mL NaOH (8%) solution. The as-so-prepared mixtures were homogenized for two hours with a magnetic stirrer. Then, the silicate solution was gradually mixed with aluminate solution in the ratio of 1:0.5 (experiment A) and 1:0.35 (experiment B). The systems were left undisturbed for 24 h at room temperature.

The feedstock gels were prepared in the same way as the seed gels but without aging. The seed gels were then mixed into the feedstock gels and put inside stainless-steel hydrothermal reactors and heated at 10 °C/min until the desired temperature (110 °C) and

kept for different times. Synthesis products were filtered with distilled water and dried in an oven at 40 °C for 24 h. The initial mixtures for experiments A and B had the following composition, respectively: 3.5 SiO_2–1.00 Al_2O_3–11 Na_2O–534 H_2O and 5.3 SiO_2–1.00 Al_2O_3–14.4 Na_2O–664 H_2O.

Powder X-ray diffraction (XRPD) analyses were performed to characterize RHA and products of synthesis; the instrument was a RIGAKU "MiniFlex II" (Rigaku, Osaka, Japan) operating with Bragg–Brentano geometry (CuKa = 1.5405 Å, 30 kV, 15 mA, 5–70° 2 theta scanning interval, step size 0.02° 2 theta, data acquisition speed of 0.033°/s). The identification of Na-P and relative peak assignment was performed with reference to the JCPDS code: 71-0962. Both the crystalline and amorphous phases in the synthesis powders were estimated using quantitative phase analysis (QPA) applying the combined Rietveld and reference intensity ratio (RIR) methods [56]; corundum NIST 676a was added to each sample, amounting to 10% (according to the strategy proposed by Novembre et al) [57] and the powder mixtures were homogenized by hand-grinding in a mortar. Data for the QPA refinement were collected in the angular range 5–70° 2 theta with steps of 0.02° and 10 s $step^{-1}$, a divergence slit of 0.5° and a receiving slit of 0.1 mm.

Data were processed with the GSAS software 3.0 [58] and the graphical interface [59] starting with the structural models proposed by Albert et al. [3] for Na-P1. The following parameters were refined: background parameters, zero shift, cell parameters, and peak profiles [60–62].

Morphological analyses were obtained by means of scanning electron microscopy, Phenom XL SEM–EDX (ThermoFisher Scientific, Dartford, UK); powders were analyzed with the following operative conditions: high vacuum, accelerating voltage of 15 kV, and 2–15 μm beam diameter.

The specific surface and porosity were obtained by applying the BET (Brunauer–Emmett–Teller) method with N_2 using a Micromeritics ASAP2010 instrument (Norcross, GA, USA) operating from 10 to 127 kPa [63].

The IR spectrum was obtained using a Shimadzu IRAffinity-1S FTIR spectrophotometer (Shimadzu Italia S.r.l., Milan, Italy) equipped with a sealed and desiccated interferometer, a DLATGS (Deuterated Triglycine Sulfate Doped with L-Alanine) detector, and a single reflection diamond ATR crystal (QATR 10, Shimadzu Italia S.r.l., Milan, Italy) [64]. The FTIR spectrum was recorded in the range of 4000–400 cm^{-1} co-adding 45 interferograms at a resolution of 4 cm^{-1} with Happ–Genzel apodization [64]. The ATR crystal was carefully cleaned before each analysis, a background was recorded for each sample and the measurements were performed in triplicate. Spectra manipulation was carried out with the software LabSolution IR version 2.27 (Shimadzu Italia S.r.l., Milan, Italy).

The Raman spectrum of NaP-1was obtained by confocal and high-performance Raman microscope XploRA PLUS (Horiba, Kyoto, Japan) with deep-cooled CCD detector technology. LabSpec 6.6.1.14 (Horiba, Kyoto, Japan) was employed to control, optimize, and process the acquired data. Furthermore, data were processed through Origin 8.5 to optimize the results. The analysis was performed in the range of 200–1200 cm^{-1} and with an 1800-line/mm grating.

Differential thermal analysis (DTA) and thermogravimetry (TG) were performed on the zeolitic powder using a Mettler TGA/SDTA851e instrument (Columbus, OH, USA) with the working conditions of 10°/min, 30–1100 °C, and a sample mass of ~10 mg in an Al_2O_3 crucible [65,66].

4. Conclusions

In this paper, we have successfully synthesized Na-P1 crystals starting from an environmentally friendly and inexpensive precursor constituted by RH. RH was pyrolyzed at 550 °C to obtain RHA. The experimental protocol of synthesis involved the mixing of a seed gel and a feedstock gel and crystallization at ambient pressure at 110 °C. Two different conditions were investigated by fixing the SiO_2/Al_2O_3 ratio at 3.5 for

experiment A and at 5.3 for experiment B. The appearance of the Na-P1 phase begins at about 24 h and the climax in the crystallization is reached at 48 h for both the experiments. Morphological study of synthetic powders reveals a ball-like shape and crystalline dimensional homogeneity (about 2 microns) for Na-P1 crystals of experiment A and different sizes (from 2 to 10 microns) and mixed morphologies (ball-like, angular and wool ball-like) for crystals of experiment B.

The complete spectrum of spectroscopic, physical, and morphological characterizations of zeolite Na-P1 synthesized starting from RHA at 48 h (experiment A) is presented here for the first time and shows that the products obtained are homogeneous in size and morphology, a factor mandatory in several industrial fields, i.e., gas separation. This demonstrates the effectiveness of the synthesis protocol by proving the validity of using RHA as a substitute for commercial silica.

Last but not least, we reached a reduction in the calcination temperature of RH and synthesis temperature. Among the authors that synthesized Na-P1 from RH [34–36], only Kongkachuichay and Lohsoontorn [36] managed to obtain the zeolite as single phase; they first pyrolyzed RH at 700 °C and then operated hydrothermal treatment at 140 °C. We have reduced calcination and hydrothermal temperatures to 550 °C and 110 °C, respectively.

Another substantial difference between our work and that of previous authors lies in the effective assessment of the degree of success of the experiment from calculation by the QPA of the percentage of crystallization vs. amorphous material and other impurities [67]. This is a fundamental requirement for an industry that claims at least 90% of pure products. Samples at 48 h of experiment A reached 93.5%.

To conclude, the comparison with the characterizations of the same zeolite obtained from traditional industrial chemical reagents suggests that transfer to an industrial production scale might be feasible.

Author Contributions: Conceptualization, D.N. and D.G.; Data curation, D.N., D.G., L.M., A.C.T., G.R., M.C. and P.d.P.; Investigation, D.N., D.G., L.M., A.C.T., G.R., M.C. and P.d.P.; Methodology, D.N. and D.G.; Supervision, D.N. and D.G.; Writing—original draft, D.N.; Writing—review and editing, D.G., L.M., A.C.T., G.R., M.C. and P.d.P. All authors have read and agreed to the published version of the manuscript.

Funding: This research received no external funding.

Informed Consent Statement: not applicable.

Data Availability Statement: The original contributions presented in this study are included in the article. Further inquiries can be directed to the corresponding author.

Acknowledgments: The authors greatly acknowledge the technical staff at the University of Barcelona (CCiT-UB) and Chieti for their help during the development of the work. M. Menéndez (Biology fac., UB) helped us with the calcination of RH.

Conflicts of Interest: The authors declare no conflicts of interest.

References

1. Nery, J.G.; Mascarenhas, Y.P.; Cheetham, A.K. A study of the highly crystalline, low-silica, fully hydrated zeolite P ion exchanged with (Mn^{2+}, Cd^{2+}, Pb^{2+}, Sr^{2+}, Ba^{2+}) cations. *Micropor. Mesopor. Mater.* **2003**, *57*, 229–248.
2. Sharma, P.; Song, J.S.; Han, M.H. GIS-NaP1 zeolite microspheres as potential water adsorption material: Influence of initial silica concentration on adsorptive and physical/topological properties. *Sci. Rep.* **2016**, *6*, 22734.
3. Albert, B.R.; Cheetham, A.K.; Stuart, J.A.; Adams, C.J. Investigations on P zeolites: Synthesis, characterization, and structure of highly crystalline low-silica NaP. *Micropor. Mesopor. Mater.* **1998**, *21*, 133–142.
4. Baerlocher, C.; Meier, W.M. The crystal structure of synthetic zeolite Na-P1, an isotope of gismondine. *Z. Krist.* **1971**, *135*, 339–354.
5. Hansen, S.; Hakansson, U.; Landa-Canovas, A.R.; Falth, L. On the crystal chemistry of NaP zeolites. *Zeolites* **1993**, *13*, 276–280.
6. Hakansson, U.; Falth, L.; Hansen, S. Structure of a high-silica variety of zeolite Na-P. *Acta Crystallogr.* **1990**, *46*, 1363–1364.

7. Adams, C.J.; Araya, A.; Cunningham, K.J.; Franklin, K.R.; White, I.F. Measurement and prediction of Ca–Na ion-exchange equilibrium in maximum aluminium P (MAP), a zeolite with the GIS framework topology. *J. Chem. Soc. Faraday Trans.* **1997**, *93*, 499–503.
8. Huo, Z.; Xu, X.; Lv, Z.; Song, J.; He, M.; Li, Z.; Wang, Q.; Yan, L.; Li, Y. Thermal study of NaP zeolite with different morphologies. *J. Therm. Anal. Calorim.* **2013**, *111*, 365–369.
9. Szala, B.; Bajda, T.; Jelen, A. Removal of Chromium (VI) from aqueous solutions using zeolites modified with HDTMA and ODTMA surfactants. *Clay Miner.* **2015**, *50*, 103–115.
10. Cocke, D. L. and Mollah, M. Y. A. The chemistry and leaching mechanisms of hazardous substances in cementitious systems. In: Chemistry and Microstructure of Solidified Waste Forms. (R. D.Spence, ed.) p.187. Lewis, Boca Raton, FL, U.S.A. (1991).
11. Atkins, M.; Glasser, F.P.; Jack, J.J. Zeolite P in cements: Its potential for immobilizing toxic and radioactive waste species. *Waste Manag.* **1995**, *15*, 127–135.
12. Li, Z.; Wu, C.; Yang, Y.; Ma, X.; Fu, L.; Peng, G.; Guan, Q.; Can, Q. Nano-Co_3O_4 supported on magnetic N-doped graphene as highly efficient catalyst for epoxidation of alkenes. *Mol. Catal.* **2017**, *432*, 267–273.
13. Mortezaei, Z.; Zendehdel, M.; Bodaghifard, M.A. Synthesis and characterization of funcionalited NaP Zeolite $CoFe_3O_4$ hybrid materials: A micro-meso-structure catalyst for aldol condensation. *Res. Chem. Intermed.* **2020**, *46*, 2169–2193.
14. Rees, L.V.C.; Chandrasekhar, S. *Verified Synthesis of Zeolitic Materials*, 2nd ed.; Robson, H., Lillerud, K.P., Eds.; Elsevier Science: Amsterdam, The Netherlands, 2001; pp. 169–170.
15. Ali, I.O.; El-Sheikh, S.M.; Salama, T.M.; Bakr, M.F.; Fodial, M.H. Controllable synthesis of NaP zeolite and its application in calcium adsorption. *Sci. China Mater.* **2015**, *58*, 621–633.
16. Li, J.T.; Zeng, X.; Chen, R.Y.; Yang, X.B.; Luo, X.T. Synthesis of pure zeolite Na-P from kaolin and enhancement of crystallization rate by sodium fluoride. In *Advanced Materials, Structure and Mechanical Engineering*; Kaloop, M., Ed.; Taylor and Francis Group: London, UK, 2016.
17. Meftha, M.; Oueslati, W.; Chorfi, N.; Ben Haj Amara, A. Effect of the raw material type and the reaction time on the synthesis of halloysite based Zeolite Na-P1. *Results Phys.* **2017**, *7*, 1475–1484.
18. Zubowa, H.L.; Kosslick, H.; Muller, D.; Richter, M.; Wilde, L.; Fricke, R. Crystallization of phase-pure zeolite NaP from MCM-22-type gel compositions under microwave radiation. *Micropor. Mesopor. Mater.* **2008**, *108*, 542–548.
19. Tayraukham, P.; Jantarit, N.; Osakoo, N.; Wittayakun, J. Synthesis of pure NaP2 zeolite from gel of NaY by conventional and microwave-assisted hydrothermal methods. *Crystals* **2020**, *10*, 951–962.
20. Sathupunya, M.; Gulari, E.; Wongkasemjit, S. ANA and GIS zeolite synthesis directly from alumatrane and silatrane by sol-gel process and microwave technique. *J. Eur. Ceram. Soc.* **2002**, *22*, 2305–2314.
21. Pal, P.; Das, J.K.; Das, N.; Bandyopadhyay, S. Synthesis of NaP zeolite at room temperature and short crystallization time by sonochemical method. *Ultrason. Sonochem.* **2013**, *20*, 314–321.
22. Srinivasan, A.; Grutzeck, M.W. The Adsorption of SO_2 by Zeolites Synthesized from Fly Ash. *Environ. Sci. Technol.* **1999**, *33*, 1464–1469.
23. Murayama, N.; Yamamoto, H.; Shibata, J. Mechanism of zeolite synthesis from coal fly ash by alkali hydrothermal reaction. *Int. J. Miner. Process.* **2002**, *64*, 1–17.
24. Kazemian, H.; Naghdali, Z.; Kashani, T.G.; Farhadi, F. Conversion of high silicon fly ash to Na-P1 zeolite: Alkaline fusion followed by hydrothermal crystallization. *Adv. Powder Technol.* **2010**, *21*, 279–283.
25. Kucuk, M.E.; Makarava, I.; Kinnarinen, T.; Hakkinen, A. Simultaneus adsorption of Cu(II), Zn(II), Cd(II) and Pb(II) from synthehticwastewater using NaP and LTA zeolites prepared from biomass fly ash. *Heliyon* **2023**, *9*, e20253.
26. Lovat, V.C.; Chandrasekhar, S. Hydrothermal reaction of kaolinite in presence of fluoride ions at pH < 10. *Zeolites* **1993**, *13*, 534–541.
27. Baccouche, A.; Srasra, E.; El Maaoui, M. Preparation of Na-P1 and sodalite octahydrate zeolites from interstratified illite-smectite. *Appl. Clay Sci.* **1998**, *13*, 255–273.
28. Kats, A.; Brough, A.R.; Kirkpatrick, R.J.; Struble, L.; Young, F. Effect of Solution Concentration on the Properties of a Cementitious Grout Wasteform for Low-Level Nuclear Waste. *Nucl. Technol.* **2017**, *129*, 236–245.
29. Sayehi, M.; Garbarino, G.; Delahay, G.; Busca, G.; Tounsi, H. Synthesis of high value-added Na-P1 and Na-FAU zeolites using waste glass from fluorescent tubes and aluminum scraps. *Mater. Chem. Phys.* **2020**, *248*, 122903.
30. Utami, A.R.; Sugiarti, S.; Sugita, P. Synthesis of NaP1 and Faujasite zeolite from natural zeolite of ENDE-NTT as lead Pb (II) adsorbent. *Rasajan J. Chem.* **2019**, *12*, 650–658.
31. Hong, S.; Um, W. Top-down synthesis of NaP zeolite from natural zeolite for the higher removal efficiency of Cs, Sr, and Ni. *Minerals* **2021**, *11*, 252.
32. Moreno-Torres, J.A.; Espejel-Ayala, F.; Ramirez-Bon, R.; Coutino-Gonzalez, E. Sustainable strategies to synthesize small-pore NaP zeolites using natural minerals. *J. Mater. Sci.* **2024**, *59*, 423–434.
33. Khabuanchalead, S.; Khemthong, P.; Prayoonpokarack, S.; Wittayakun, J. Transformation of zeolite NaY synthesized from rice husk silica to NaP during hydrothermal synthesis. *J. Sci. Technol.* **2008**, *15*, 225–231.
34. Wittayakun, J.; Khemthong, P.; Prayoonpokarach, S. Synthesis and characterization of zeolite NaY fron rice husk silica. *Korean J. Chem. Eng.* **2008**, *25*, 861–864.
35. Mohamed, R.M.; Mkhalid, I.A.; Bakarat, M.A. Rice husk ash as a renewable source for the production of zeolite NaY and its characterization. *Arab. J. Chem.* **2015**, *8*, 48–53.

36. Kongkachuichay, P.; Lohsoontorn, P. Phase diagram of zeolite synthesized from perlite and rice husk ash. *ScienceAsia* **2006**, *32*, 13–16.
37. Vasconcelos, A.A.; Len, T.; de Nararé Oliveira, A.; da Farias Costa, A.A.; da Silva Souza, A.R.; da Ferreira Costa, C.E.; Luque, R.; da Rocha Filho, G.N.; Rodriguez Noronha, R.C.; do Santos Nascimento, L.A. Zeolites: A Theoretical and Practical Approach with Uses in (Bio) Chemical Processes. *Appl. Sci.* **2023**, *13*, 1897–1951.
38. Akinjokun, A.I.; Ogunfowokan, A.O.; Ajao, J.; Petrik, L.F.; Ojumu, T.V. Template-free conversion of rice husk silica into nano-zeolite X and its application in adsorption of heavy metal ions. *Int. J. Environ. Sci. Technol.* **2024**, *21*, 1949–1960.
39. Treacy, M.M.J.; Higgins, J.B.; Ballmoos, R. *Collectionof Simulated XRD Powder Patterns for Zeolites*, 3rd ed.; Elsevier: Amsterdam, The Netherlands, 1996.
40. Petkowicz, D.I.; Rigo, R.T.; Radtke, C.; Pergher, S.B.; dos Santos, J.H.Z. Zeolite NaA from Brazilian Chrysotile and rice husk. *Micropor. Mesopor. Mater.* **2008**, *116*, 548–554.
41. Yusof, A.M.; Malek, N.A.N.N.; Rashid, N.A.A. Hydrothermal conversion of rice husk ash to faujasite-types and NaA-type of zeolites. *J. Porous. Mater.* **2010**, *17*, 39–47.
42. Novembre, D.; Gimeno, D.; Marinangeli, L.; Tangari, A.C.; Rosatelli, G.; Ciulla, M.; di Profio, P. Rice Husk as Raw Material in Synthesis of NaA (LTA) Zeolite. *Molecules* **2024**, *29*, 4396.
43. Breck, D. *Zeolite Molecular Sieves*; John Wiley & Sons: New York, NY, USA, 1974.
44. Flanigen, E.M.; Khatami, H.; Szymanski, H.A. Infrared Structural Studies of Zeolite Frameworks. In *Molecular Sieve Zeolites, Advances in Chemistry 101*; Flanigen, E.M., Sand, L.B., Eds.; American Chemical Society: Washington, DC, USA, 1971; pp. 201–229.
45. Novembre, D.; Gimeno, D.; Del Vecchio, A. Synthesis and characterization of Na-P1 (GIS) zeolite using a kaolinitic rock. *Sci. Rep.* **2021**, *11*, 4872–4883.
46. Tsai, Y.L.; Huang, E.; Li, Y.H.; Hung, H.T.; Jiang, J.H.; Liu, T.C.; Fang, J.N.; Chen, H.F. Raman spectroscopic characteristics of Zeolite Group Minerals. *Minerals* **2021**, *11*, 167.
47. Mozgawa, W. The relation between structure and vibrational spectra of natural zeolites. *J. Mol. Struct.* **2001**, *596*, 129–137.
48. Novembre, D.; Gimeno, D.; Pasculli, A.; Di Sabatino, B. Synthesis and characterization of sodalite using natural kaolinite: An analytical and mathematical approach to simulate the loss in weight of chlorine during the synthesis process. *Fresen. Environ. Bull.* **2010**, *19*, 1109–1117.
49. Novembre, D.; Pasculli, A.; Pace, C.; Gimeno, D.; Di Sabatino, B. Synthesis of sodalite from natural kaolinite. A way to simulate the loss in weight of chlorine during synthesis process by an analytical and mathematical modelling. *Rend. Online Soc. Geol. It.* **2010**, *11*, 548–549.
50. Novembre, D.; Gimeno, D.; D'Alessandro, N.; Tonucci, L. Hydrothermal synthesis and characterization of kalsilite by using a kaolinitic rock from Sardinia, Italy, and its application in the production of biodiesel. *Mineral. Mag.* **2018**, *82*, 961–973.
51. Gisbert, G.; Gimeno, D. Ignimbrite correlation using whole-rock geochemistry: An example from the Sulcis (SW Sardinia, Italy). *Geol. Mag.* **2017**, *154*, 740–756.
52. Novembre, D.; Di Sabatino, B.; Gimeno, D.; Garcia Valles, M.; Martinez-Manent, S. Synthesis of Na-X zeolites from tripolaceous deposits (Crotone, Italy) and volcanic zeolitized rocks (Vico Volcano, Italy). Micropor. Mesopor. Mat. **2004**, 75, 1–11.
53. Aulinas, M.; Civetta, L.; Di Vito, M.; Orsi, G.; Gimeno, D.; Fernandez Turiel, J.L. The Plinian Mercato eruption of Somma Vesuvius: Magma chamber processes and eruption dynamics. *Bull. Volcanol.* **2008**, *70*, 825–840.
54. Gimeno, D.; Puges, M. Caracterización química de la vidriera histórica de Sant Pere i Sant Jaume (Monestir de Pedralbes, Barcelona). *Bol. Soc. Esp. Ceram. Vidr.* **2002**, *41*, 13–20.
55. Aulinas, M.; Gimeno, D.; Fernandez-Turiel, J.L.; Perez-Torrado, F.J.; Rodriguez-Gonzalez, A.; Gasperini, D. The Plio-Quaternary magmatic feeding system beneath Gran Canaria (Canary Islands, Spain): Constraints from thermobarometric studies. *J. Geol. Soc.* **2010**, *167*, 785–801.
56. Novembre, D.; Pace, C.; Gimeno, D. Syntheses and characterization of zeolites K-F and W type using a diatomite precursor. Mineral. Mag. 2014, 78, 1209–1225.
57. Novembre, D.; Gimeno, D.; Del Vecchio, A. Improvement in the synthesis conditions and studying the physicochemical properties of the zeolite Li-A (BW) obtained from a kaolinitic rock. *Sci. Rep.* **2020**, *10*, 5715–5723.
58. Novembre, D.; Pace, C.; Gimeno, D. Synthesis and characterization of wollastonite-2M by using a diatomite precursor. *Mineral. Mag.* **2018**, *82*, 95–110.
59. Larson, A.C.; Von Dreele, R.B. GSAS: General Structure Analysis System. In *Document Laur 86-748*; Los Alamos National Laboratory: Los Alamos, NM, USA, 1997.
60. Toby, B.H. EXPGUI, a Graphical User Interface for GSAS. *J. Appl. Crystallogr.* **2001**, *34*, 210–213.
61. Novembre, D.; Gimeno, D. The solid-state conversion of kaolin to $KAlSiO_4$ minerals: The effects of time and temperature. *Clays Clay Miner.* **2017**, *65*, 355–366.
62. Novembre, D.; Gimeno, D.; Poe, B. Synthesis and Characterization of Leucite Using a Diatomite Precursor. *Sci. Rep.* **2019**, *9*, 10051–10061.
63. Novembre, D.; Gimeno, D.; Cappelletti, P.; Graziano, S.F. A case study of zeolitization process: "tufo Rosso a Scorie Nere" (Vico Volcano, Italy): Inferences for a general model. *Eur. J. Mineral.* **2021**, *33*, 315–328.
64. Novembre, D.; Di Sabatino, B.; Gimeno, D. Synthesis of Na-A zeolite from 10 Å halloysite and a new crystallization kinetic model for the transformation of Na-A into HS zeolite. *Clays Clay Miner.* **2005**, *53*, 28–36.

65. Ciulla, M.; Canale, V.; Wolicki, R.D.; Pilato, S.; Bruni, P.; Ferrari, S.; Siani, G.; Fontana, A.; Di Profio, P. Enhanced CO_2 Capture by Sorption on Electrospun Poly (Methyl Methacrylate). *Separations* **2023**, *10*, 505–521.
66. Novembre, D.; Di Sabatino, B.; Gimeno, D.; Pace, C. Synthesis and characterization of Na-X, Na-A and Na-P zeolites and hydroxysodalite from metakaolinite. *Clay Miner.* **2011**, *46*, 336–354.
67. Novembre, D.; Gimeno, D. Synthesis and characterization of analcime (ANA) zeolite using a kaolinitic rock. *Sci. Rep.* **2021**, *11*, 13373–13382.